

Pyrolytic-deoxygenation of triglyceride via natural waste shell derived Ca(OH)₂ nanocatalyst



N. Asikin-Mijan^{a,b}, H.V. Lee^{a,*}, Y.H. Taufiq-Yap^{b,*}, J.C. Juan^{a,c}, N.A. Rahman^d

^a Nanotechnology & Catalysis Research Centre (NanoCat), Institute of Postgraduate Studies University Malaya, 50603 Kuala Lumpur, Malaysia

^b Catalysis Science and Technology Research Centre (PutraCat), Faculty of Science, Universiti Putra Malaysia, 43400 UPM Serdang, Selangor, Malaysia

^c School of Science, Monash University, Sunway Campus, Jalan Lagoon Selatan 46150, Selangor, Malaysia

^d Environmental Research Group, Department of Chemistry, Faculty of Science, University of Malaya, 50603 Kuala Lumpur, Malaysia

ARTICLE INFO

Article history:

Received 27 April 2015

Received in revised form

15 December 2015

Accepted 22 December 2015

Available online 29 December 2015

Keywords:

Cracking

Decarboxylation-decarbonylation

Calcium oxide

Clamshell

Hydrocarbon

ABSTRACT

Cracking-Deoxygenation process is one of the important reaction pathways for the production of biofuel with desirable *n*-C₁₇ hydrocarbon chain via removal of oxygen compounds. Calcium-based catalyst has attracted much attention in deoxygenation process due its relatively high capacity in removing oxygenated compounds in the form of CO₂ and CO under decarboxylation and decarbonylation reaction, respectively. In the present study, deoxygenation of triolein was investigated using Ca(OH)₂ nanocatalyst derived from low cost natural waste shells. The Ca(OH)₂ nanocatalyst was prepared via integration techniques between surfactant treatment (anionic and non-ionic) and wet sonochemical effect. Results showed that sonochemically assisted surfactant treatment has successfully enhanced the physicochemical properties of Ca(OH)₂ nanocatalyst in terms of nano-particle sizes (~50 nm), high surface area (~130 m² g⁻¹), large porosity (~18.6 nm) and strong basic strength. The presence of superior properties from surfactant treated Ca(OH)₂ nanocatalysts rendered high deoxygenation degree, which are capable of producing high alkane and alkene selectivity in chain length of *n*-C₁₇ (high value of C₁₇/*n*-C₁₇ + *n*-C₁₈) ratio = 0.88). Furthermore, both Ca(OH)₂-EG and Ca(OH)₂-CTAB nanocatalysts showed high reactivity with 47.37% and 44.50%, respectively in total liquid hydrocarbon content of triolein conversion with high H/C and low O/C ratio.

© 2015 Elsevier B.V. All rights reserved.

1. Introduction

Recently, concern of climate change had triggered the development of economical friendly and sustainable biofuel for the future of energy and fuel production [1]. Biodiesel had attracted much attention by many researchers [2]. However, this first generation biofuel energy has several disadvantages. In December 2014, the world's first Boeing flight (ecoDemonstrator 787) using "green diesel" took off, however, it showed that pure biodiesel (B100) was not suitable to be used as aviation fuel as it contained high oxygen content (less stable), which could cause serious damage to the engine plug, filter, and corrosion to the metal parts in long term operation [3,4,5]. Other incompatibility included poor storability, immiscibility with gasoline [6], high cloud point and other engine compatibility issues. Hence, reduction of oxygenated

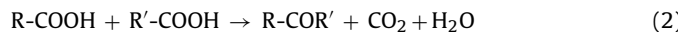
compound is a key factor in improving fuel stability. Numerous technologies for hydrocarbon biofuel production have been developed such as hydrodeoxygenation [7–9] and deoxygenation process [10–12]. Hydrodeoxygenation (HDO) is a hydrogenolysis reaction to remove oxygen from oxygennated compounds (ester and carbonyl groups) with the presence of H₂ gas and resulting in by-product (H₂O) formation. In contrast to the HDO process, deoxygenation (DO) reaction involved the removal of oxygen via cracking-decarboxylation pathway by release of CO and CO₂ gaseous without H₂ consumption [13]. Even though hydrodeoxygenation process is the most efficient method for high quality liquid hydrocarbon production. However, the inflated production cost due to hydrogen consumption is an sustainability issue. Therefore, many researchers focused on deoxygenation technique which requires no hydrogen gas.

Selective catalytic deoxygenation of triglyceride via base-catalyze cracking-decarboxylation mechanism has been an active area of recent research in order to reduce the production cost. According to literature study, heterogeneous basic catalysts can be employed for the production of liquid hydrocarbon fuel by means

* Corresponding author. Fax: +60 3 7957 6956.

E-mail addresses: leehweivoon@um.edu.my (H.V. Lee), taufiq@upm.edu.my (N.A. Rahman).

of deoxygenation of low quality biomass feedstock oil (oxygenated oil). Gomez et al. showed that the catalytic deoxygenation of methyl octanoate has successfully conducted with high activity (85%) and selectivity to the desired hydrocarbon products (80%) in the presence of high basic strength of K-zeolite and Cs-zeolite catalysts [14]. Besides, it was found that MgO-supported catalyst promoted the decarboxyl-cracking of palm oil and other triglyceride to make middle-distillate range hydrocarbons (mixture of olefins and paraffin) at 430 °C. The basicity of supported MgO is capable to reduce the acid value and iodine value, which is suitable to be used for the diesel engine [15]. Ding's research group (2009) has successfully converted organic acid (naphthenic acid), which are naturally occurring compounds in petroleum into hydrocarbon chain products by using CaO catalyst. With the presence of CaO, multiple pathways (catalytic decarboxylation, neutralization, and thermal cracking) were responsible for the naphthenic acid (NA) conversion [16]. Furthermore, Lin et al. claimed that CaO catalyst could absorb more CO₂ either in gas phase or liquid phase, which simultaneously remove the oxygen molecule via decarboxylation and decarbonylation mechanism [17]. Therefore, CaO is a potential catalyst for catalytic deoxygenation reaction. Equation below showed CaO catalysed deoxygenation of acid compound [9]:



Several studies had reported that calcium hydroxide (Ca(OH)₂) is capable of rendering better reactivity and product selectivity compared to CaO catalyst [18,19]. It is due to the presence of enhanced superior properties such as basicity and textural properties (surface area, pore volume, pore diameter) of Ca(OH)₂ especially in nanoparticles sizes [20,21]. Ca(OH)₂ can be derived from waste natural shell, which is the common sources of calcium carbonate [22]. The waste shell can be easily converted into Ca(OH)₂ phases by using water hydroxylation treatment. Natural waste shell derived Ca(OH)₂ can be considered as a low cost green solid base catalyst which was enhanced for deoxygenation reaction. Nevertheless, there is no literature report pertaining nano-sizes of Ca(OH)₂ derived from waste shell for hydrocarbon biofuel production.

Thus, in the present study, we have investigated the feasibility of nano-Ca(OH)₂ derived from waste clamshell (*Meretrix meretrix* sp.) for deoxygenation of triglyceride via decarboxylation and decarbonylation mechanism. Waste clamshell-derived Ca(OH)₂ nanoparticles was prepared by using sonochemical assisted wet surfactant treatment, where different type of surfactant (ionic and non-ionic surfactant) was tested. The physiochemical properties of prepared catalysts were characterized by using XRF, XRD, BET, TPD-CO₂, SEM and TEM analysis. Furthermore, the effect of deoxygenation efficiency from Ca(OH)₂ nanoparticles catalyzed reaction was investigated. The final deoxygenized liquid product was analyzed by using FTIR and GC-MS for chemical composition study. Besides, CHNOS analysis was used to determine the oxygen composition in final deoxygenized liquid product.

2. Experimental

2.1. Material

Washed natural waste clamshell (*Meretrix meretrix* sp.) was used as described in [20]. Triolein was obtained from sigma aldrich. Ethylene glycol (99.8%, Merck) and *N*-Cetyl-*N,N,N*-trimethylammonium bromide (98%, R&M chemical) was used as surfactant. Commercial Ca(OH)₂ nano-powder (>99.8%, Sigma Aldrich), and commercial CaO powder (99.9%, R&M chemical) was used for comparison study.

Gas Chromatography (GC) grade *n*-Hexane for GC-MS analysis with purity > 98% was purchased from Merck.

2.2. Catalyst synthesis

Waste clamshell powder (~300 μ) was thermally activated at 800 °C for 2 h under atmosphere conditions and denoted as CaO. Clamshell-derived CaO was then underwent sonochemical assisted wet surfactant treatment, where the combusted clamshell was added into ethylene glycol (EG) solution (1 M) and *N*-Cetyl-*N,N,N*-trimethylammonium bromide (CTAB) solution (1 M), respectively under 60 Hz to achieve uniform size of nanoparticles followed by aging for 5 h in room temperature. The medium was filtered with PTFE membrane filters and washed with mixture of distilled water and ethanol (1:1 ratio) for several times (1000 ml of solution) before it was dried in the oven overnight at 100 °C. Lastly, the precursors were calcined at 400 °C for 2 h for final catalyst activation. The calcined samples that treated with EG, CTAB and water are denoted as Ca(OH)₂-EG, Ca(OH)₂-CTAB and Ca(OH)₂-H₂O, respectively.

2.3. Catalyst characterization

Elemental analysis of the samples was analyzed by using X-ray fluorescence (XRF) spectrometry (Philips PWI404) equipped with a scandium anode tube. The crystalline phases of calcined samples were analyzed by X-ray diffractometer (Shimadzu diffractometer model XRD-6000). The surface area and pore volume of the samples were determined by Brunauer–Emmet–Teller (BET) model by using Thermo–Finnigan Sorpmatic 1990 series. The samples were degassed overnight at 150 °C in vacuum. The chemical properties of catalysts was evaluated using temperature programme desorption CO₂ (Thermo Finnigan TPD/R/O 1100) equipped with a thermal conductivity detector (TCD). Approximately, 0.05 g of catalyst was treated under N₂ gas flow for 30 min at 250 °C. Then, the catalyst was exposed to CO₂ gas for 60 min at ambient temperature to allow adsorption of CO₂ on the surfaces. The excess of CO₂ were subsequently flushed out by flowing N₂ gas prior to the analysis. Desorption of the CO₂ from the basic sites of the catalyst were identified by TCD under helium gas (30 ml/min) ranging from 50 °C to 900 °C. Morphological and particle size of the catalyst was investigated by scanning electron microscopy (SEM) (SEM JOEL 6400) and transmission electron microscopy (TEM) (Hitachi H-7100 TEM) with accelerating voltage of 10 mV.

2.4. Catalytic cracking-deoxygenation of triolein

The deoxygenation reaction of triolein were carried out at temperature of 350 °C under partial vacuum condition (10 mbar) for 30 min [23]. Approximately 10 g of triolein and clamshell derived catalyst (5 wt.%) was added into 250 ml of batch reactor equipped with distillation and vacuum system (Fig. 1). Cold water flow in distillation system was used to promote condensation of deoxygenized species into liquid form. The fractions of deoxygenated product was further analysed by using FTIR, GC-MS and CHNOS analyser. All the reaction was repeated for three times in order to achieve precise and accurate readings.

2.5. Analysis of deoxygenized products

FTIR analysis was performed using Perkin-Elmer Spectrum (PS) 100 FT-IR spectrometer with resolution of 4 cm⁻¹ operating in the range of 300–4000 cm⁻¹. This analysis helps to determine the chemical functional group of the liquid product. The distribution of deoxygenized products were further qualitatively and quantitatively determined using GC-MS (SHIMADZU QP2010) equipped

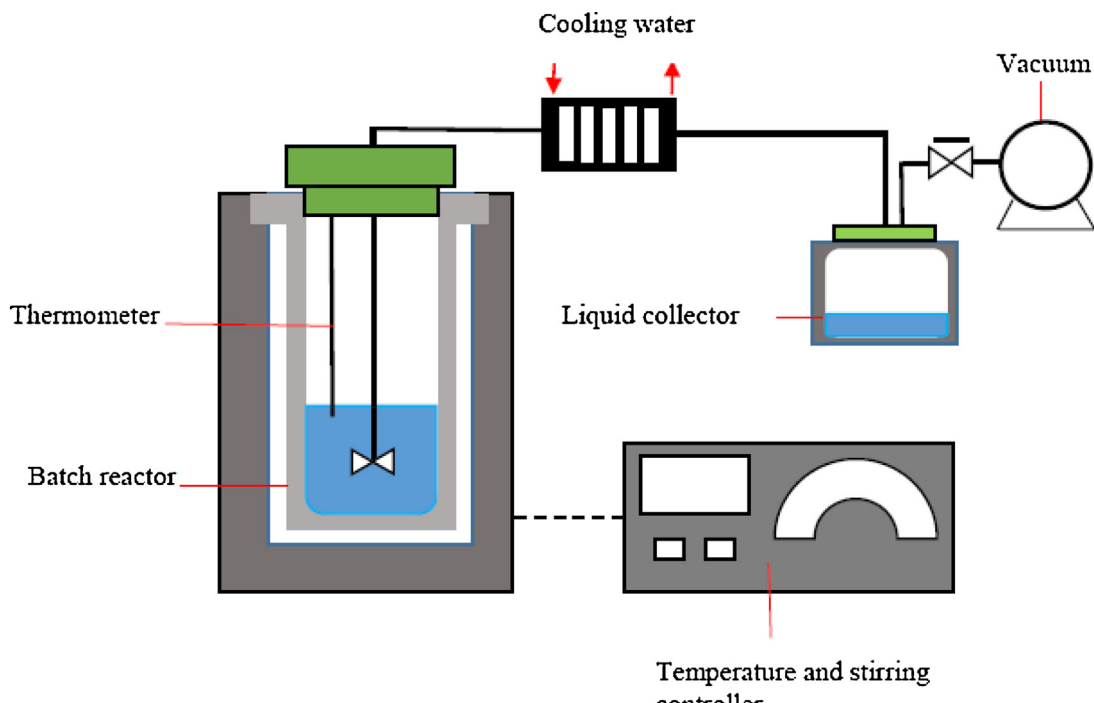


Fig. 1. Schematic diagram of deoxygenation reactor for cracking-decarboxylation/decarbonylation process.

with non-polar BPX-5 column ($12\text{ m} \times 0.53\text{ mm I.D } \mu\text{m}$ film thickness) in split mode. The fraction peaks obtained from mass spectra were identified using the National Institute of Standards and Testing (NIST) library. Furthermore, catalytic activity of different catalysts towards deoxygenation (Total product yield and product selectivity) was determined by comparing the peak area % of obtained spectra. It is known that the GC-MS analysis does not provide exact quantitative analytic result of compounds. However, it is possible to compare the product yield and product selectivity by comparing the peak areas as the chromatographic peak area of compounds is proportional to its quantity and the relative content of the product (Eq. (1) and Eq. (2) [24–26]. In order to confirm the reproducibility of the results, the experiments were conducted for three times, with the average of the peak area and peak area % was calculated. Besides, degree of oxygen to carbon molar ratio and degree of hydrogen to carbon molar ratio are shown in eq. 3 and Eq. (4) [27], respectively.

$$\text{Product Yield (\%)} = \frac{\text{Area of } C_6-C_{24}}{\text{Total area of the product}} \times 100\% \quad (1)$$

$$\text{Product Selectivity (\%)} = \frac{\text{Area of the desired product}}{\text{Total area of the product}} \times 100\% \quad (2)$$

Degree of oxygen to carbon molar ratio:

$$\text{Oxygentocarbon } \left(\frac{O}{C} \right) = \frac{\text{Oxygen content}}{\text{Carbon content}} \quad (3)$$

Degree of hydrogen to carbon molar ratio:

$$\text{Hydrogentocarbon } \left(\frac{H}{C} \right) = \frac{\text{Hydrogen content}}{\text{Carbon content}} \quad (4)$$

3. Results and discussion

3.1. X-ray fluorescence (XRF)

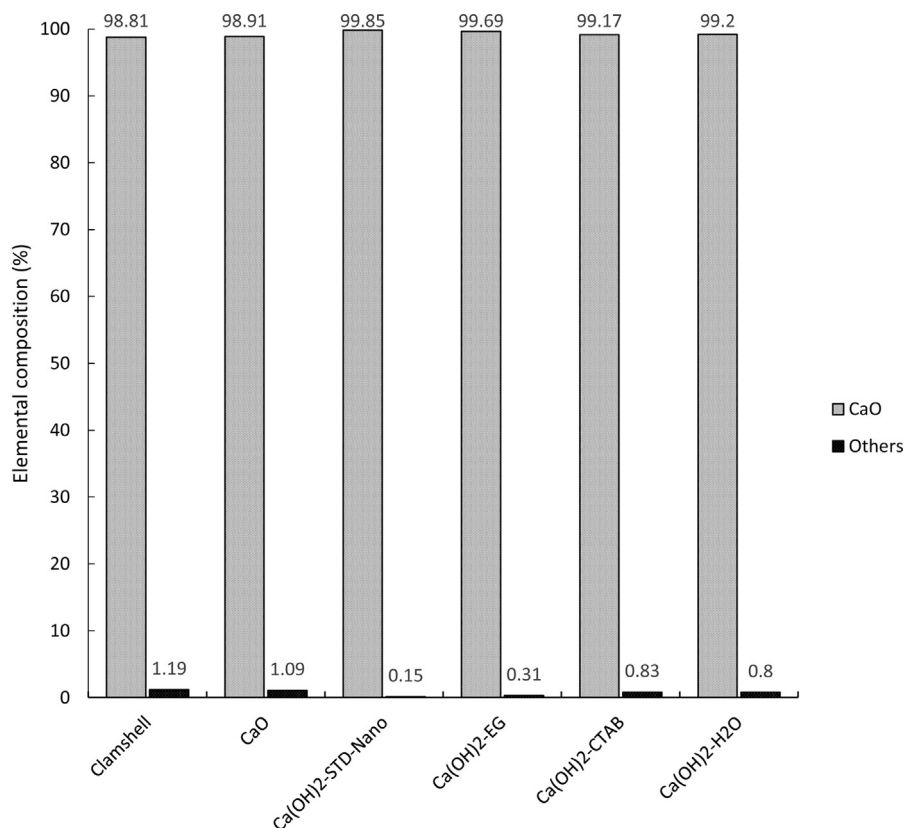
The elemental compositions of the clamshell, combusted clamshell and surfactant treated products are shown in Fig. 2.

CaO derived from waste clamshell showed high calcium content (98.81%), which indicated that the clamshell is a potential calcium resource for CaO catalyst preparation. The Ca content for surfactant treated samples $\text{Ca(OH)}_2\text{-EG}$, $\text{Ca(OH)}_2\text{-CTAB}$, and $\text{Ca(OH)}_2\text{-H}_2\text{O}$ are maintained after calcined at 400°C . This implies that the sonochemical method coupled with surfactant did not digest the calcium species from clamshell. It is also clear that there is no interfacial reaction occurred between the calcium species and surfactant during ultrasonication process, which could drastically change the composition of treated samples.

3.2. X-ray diffraction (XRD)

Fig. 3 shows the typical calcium carbonate (CaCO_3) phases at $2\theta=26.2^\circ$, 29.5° , 33.1° , 45.8° and 48.3° (JCPDS card no. 00-001-1033) from waste clamshell. The carbonate phases were successfully converted to oxide phases at temperature of 900°C as reported in previous study [20]. Minor peak of CaCO_3 at 29.4° were observed in all Ca(OH)_2 samples indicated the adsorption of CO_2 gas from the atmosphere to the active sites of catalyst. The ultrasonic-wet surfactant treated samples ($\text{Ca(OH)}_2\text{-EG}$, $\text{Ca(OH)}_2\text{-CTAB}$) and non-surfactant treated $\text{Ca(OH)}_2\text{-H}_2\text{O}$ exhibited Ca(OH)_2 phases at $2\theta=18.14^\circ$, 28.7° , 34.2° , and 50.8° (Portlandite, JCPDS card no. 00-002-0968). This showed that Ca(OH)_2 catalysts was successfully synthesized from clamshell materials. From the XRD patterns, it was observed that the crystallinity of nano- Ca(OH)_2 treated with ethylene glycol (EG) was lower compared to CTAB and water treated catalyst. This demonstrated that wet sonochemical with non-ionic surfactant of ethylene glycol has the tendency to reduce the growth of crystallite size compared to cationic surfactant (CTAB). The EG surfactant was efficiently coated on the surface of Ca(OH)_2 particles and thus prevented aggregation during calcination [28,29]. Furthermore, the presence of ultrasonic effect has further enhanced the dispersibility between sample's particles and surfactant.

Crystallite size profile of clamshell derived CaO and Ca(OH)_2 with different wet surfactant treatment are shown in Table 1. The



*other minor content of metal oxide are SrO, Fe₂O₃, CuO, Ho₂O₃, SO₃ and K₂O

Fig. 2. Elemental composition of fresh clamshell, CaO, Ca(OH)₂-STD-Nano, Ca(OH)₂-EG, Ca(OH)₂-CTAB and Ca(OH)₂-H₂O.

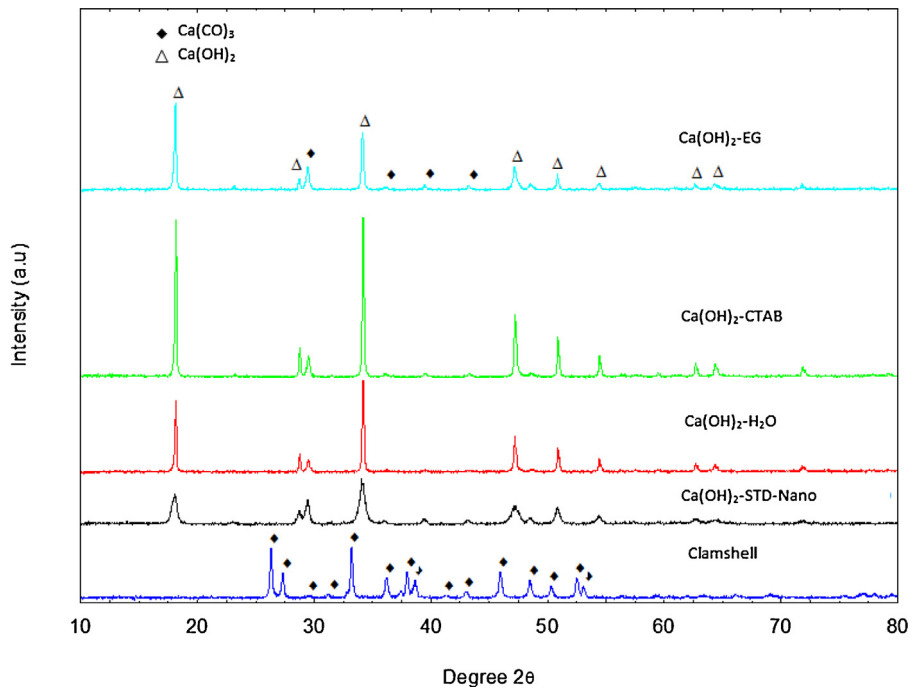


Fig. 3. XRD analysis for clamshell, CaO, Ca(OH)₂-STD-Nano, Ca(OH)₂-EG, Ca(OH)₂-CTAB and Ca(OH)₂-H₂O.

treated catalysts rendered significant reduction of crystallite sizes compared to clamshell derived CaO, which reduces in the order of Ca(OH)₂-EG < Ca(OH)₂-CTAB < Ca(OH)₂-H₂O. This implied that

sonochemical method coupled with surfactant and wet-sonication treatment has efficiently controlled the crystallite size of Ca(OH)₂.

Table 1

Crystallite sizes and textural properties profile of CaO, Ca(OH)₂–STD–Nano, Ca(OH)₂–H₂O, Ca(OH)₂–EG, Ca(OH)₂–CTAB.

Catalyst	^a Crystallite size (nm)	^b Surface area (m ² /g)	^b Pore size diameter range (nm)
CaO	68.2	11	0.2
Ca(OH) ₂ –STD–Nano	17.3	84	0.3
Ca(OH) ₂ –H ₂ O	47.8	80	18.4
Ca(OH) ₂ –EG	39.6	130	18.3
Ca(OH) ₂ –CTAB	57.2	124	18.6

^aMeasured by using Scherer equation from XRD data (repeated twice).

^bDetermined by BET analysis (repeated twice).

Table 2

Temperature programme–carbon dioxide (TPD–CO₂) profile of catalysts.

Catalyst	CO ₂ desorption temperature (°C)	Amount of CO ₂ desorbed (μmol/g)
CaO	634	554.87
Ca(OH) ₂ –STD–Nano	718	3335.82
Ca(OH) ₂ –H ₂ O	660	1133.41
Ca(OH) ₂ –EG	728	4658.77
Ca(OH) ₂ –CTAB	776	7556.38

3.3. Brunauer–Emmet–Teller surface area measurement (BET)

Table 1 shows the BET surface area of CaO ($10.90\text{ m}^2\text{ g}^{-1}$) has drastically increased up to $130\text{ m}^2\text{ g}^{-1}$, $124\text{ m}^2\text{ g}^{-1}$ and $80\text{ m}^2\text{ g}^{-1}$ for Ca(OH)₂–EG, Ca(OH)₂–CTAB and Ca(OH)₂–H₂O, respectively, after being treated with surfactant–sonochemical process. The integration of surfactants (EG or CTAB) coupled with wet–sonochemical method was capable of increasing the surface area of Ca(OH)₂ by 55–62%. Furthermore, the presence of ultrasonic effectively dispersed the large aggregates of Ca(OH)₂, while adding of surfactant has avoided the formation of big aggregates during drying and calcination process. The collapse of the cavitations bubbles generated during sonication has led to the pitting and erosion on the newly formed of Ca(OH)₂ catalyst surface [30] and thus high porosity was formed on the catalyst.

3.4. Temperature programme desorption–carbon dioxide (TPD–CO₂)

The basicity profile of catalysts was investigated by using TPD–CO₂ analysis (**Fig. 4** and **Table 2**). The basic strength distribution from catalyst's active sites is expressed in terms of CO₂ desorption temperature. The TPD–CO₂ desorption patterns (**Fig. 4**) showed different desorption peaks at different temperature, where CO₂ desorption at 100 – 500°C assigned as interaction of CO₂ with sites of weak and medium basic strengths [31]. Whereas, the CO₂ desorbed at temperature of $\sim 600^\circ\text{C}$ can be attributed an involvement of the stronger basic sites [32,33]. Based on the results, the sonochemically assisted surfactant treated catalysts exhibit stronger of basic strength and higher amount of basicity than the waste shell derived CaO and standard nano–Ca(OH)₂. The trend of the basicity was as follow Ca(OH)₂–CTAB > Ca(OH)₂–EG > Ca(OH)₂–STD–Nano > Ca(OH)₂–H₂O > CaO. The increased basicity of treated catalysts was due to the presence of Lewis and Bronsted basic sites after going through the hydration–dehydration pathway. Furthermore, the presence of high surface area of basic active sites has indicated the increment of active basic sites of treated catalysts.

3.5. Scanning electron microscopy (SEM)

SEM images for all catalysts are shown in **Fig. 5**. The surface morphology and the microstructure of the starting material, CaO derived from clamshell, Ca(OH)₂–STD–Nano, treated surfactant catalysts (Ca(OH)₂–EG, Ca(OH)₂–CTAB) and water treated sample (Ca(OH)₂–H₂O) was found to be varied. CaO (**Fig. 5a**) rendered

large and irregular shape of particles compared to standard nano–Ca(OH)₂ (**Fig. 5b**) and treated catalysts (**Fig. 5c** and d). SEM images showed that the structure and particle shapes were different based on the nature of surfactant used. EG treated catalyst showed the presence of rod crystal particles while CTAB treated catalyst has round crystal structures. Furthermore, it is significantly observed that the particle sizes of treated catalysts were significantly smaller compared to catalyst without treatment.

3.6. Transmission electron microscopy (TEM)

TEM images showed that initial shape of waste shell-derived CaO appeared in irregular aggregates forms had changed to cubic-like nanostructures after being treated with surfactants in the presence of sonication effect (**Fig. 6**). Results showed that the treated catalysts (Ca(OH)₂–EG and Ca(OH)₂–CTAB) rendered comparable of particle sizes to standard nano–Ca(OH)₂. It was anticipated that the treated nano-catalysts with high textural properties and highly amount of active sites are capable of performing more efficiently in cracking–decarboxylation reaction.

3.7. Catalytic activity study

3.7.1. Chemical composition profile of deoxygenized product

FTIR analysis was performed in order to study the chemical functional group exhibited in deoxygenized product (**Fig. 7**). The FTIR spectra for triolein showed three main absorption band at 2950 , 1741 and 1150 cm^{-1} , which attributed to stretching absorption of the C–H bond attached to the cis-carbon atom in the oleic acid moieties, absorption of glyceride carbonyl group ($-\text{C=O}$) and C–O–C group from ester bond, respectively. Results showed that reacted products rendered a new peak at $\sim 2919\text{ cm}^{-1}$, which indicated merging of two $-\text{CH}_2$ absorption bands of triolein. This resulted in shifting of $-\text{CH}_2$ (symmetrical stretching) in triolein into $-\text{CH}_2$ of asymmetrical stretching. Furthermore, slight shift of FTIR peaks ($\sim 1710\text{ cm}^{-1}$) of deoxygenized product has indicated $-\text{C=O}$ of carboxylic acid group [34]. Similar case occurred at absorption bands of $-\text{CH}_2$ ($\sim 1455\text{ cm}^{-1}$) and $-\text{CH}_3$ ($\sim 1372\text{ cm}^{-1}$) from triolein, where a new peak was appeared at 1448 cm^{-1} ($-\text{CH}_2$ bending in aliphatic) after deoxygenation reaction. This was in agreement with the formation of CC bond of alkyl chain in hydrocarbon compounds that observed at 1265 – 1281 cm^{-1} , which agreed to the occurrence of deoxygenation reaction.

3.7.2. Oxygen removal rate

Elemental analysis for oxygen, carbon and hydrogen content of deoxygenized product was determined via CHNOS analyser. The results were depicted in terms of H/C and O/C ratio in Kremel diagram (**Fig. 8**). The H/C and O/C ratio of triolein was 0.1801 and 0.3139 , respectively, which consisted highest amount of oxygen content. Interestingly, all the products from deoxygenation reaction rendered reduction of O/C ratio, which indicated oxygen compounds were removed via decarbonylation or decarboxylation process. Although deoxygenized product from blank experiment (without catalyst) showed reduction of oxygen content, however

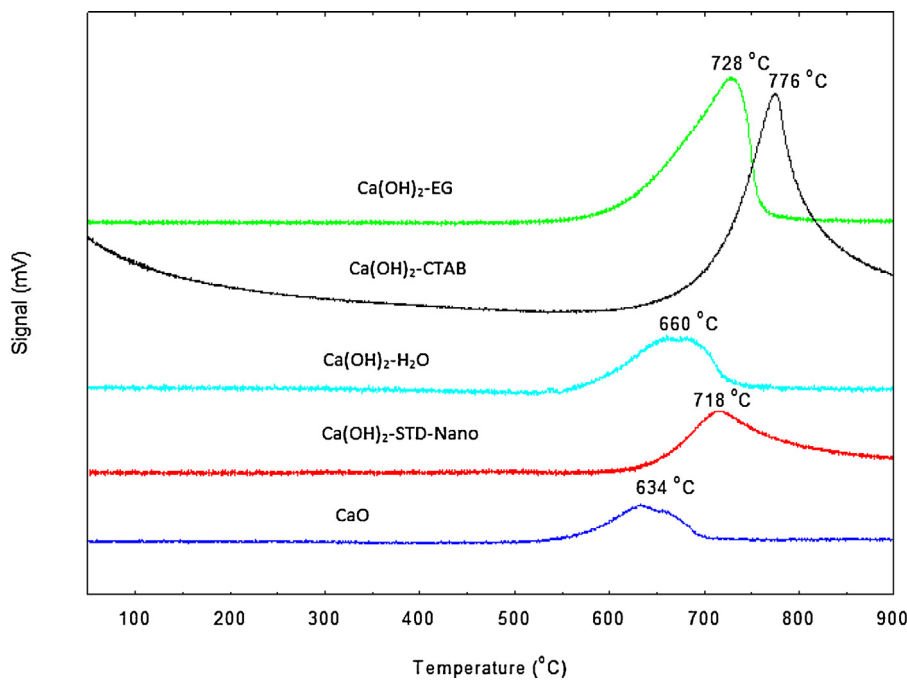


Fig. 4. TPD–CO₂ analysis for CaO, Ca(OH)₂–STD-Nano, Ca(OH)₂–EG, Ca(OH)₂–CTAB and Ca(OH)₂–H₂O.

the reaction prone to high cracking effect that caused the formation of shorter carbon chain compounds with low saturated chain (H/C ratio = 0.159). Similar case with CaO catalysed deoxygenation reaction, where low H/C ratio (0.157) resulted in undesired light hydrocarbon products. Alternatively, the treated catalysts (Ca(OH)₂–EG and Ca(OH)₂–CTAB) and standard nano-Ca(OH)₂ rendered decrement in oxygen content, while maintained H/C ratio as triolein. In the absence of H₂ condition, oxygen tends to be removed in the form of CO₂ or CO gases without addition of hydrogen atom, which might yield most of alkene compounds. This is in agreement with Lin's research study where the oxygen content significantly decreased in the presence of Ca-based catalyst. Moreover, Ca-based catalyst are capable of absorbing CO₂ efficiently from the feeds and enhancing the oxygen removal [17]. Kim's group reported that the presence of H₂ gas in hydrodeoxygenation process would reduce unsaturated bond of alkene compounds into alkanes products, and thus increase the hydrogen content (H/C) of final product [35].

3.7.3. Chemical composition study of deoxygenized liquid

The degree of selectivity for each catalyst toward *n*-alkane and *n*-alkene obtained from the deoxygenation reaction was determined by using GC–MS analysis. Table 3 showed the total composition of *n*-alkane and *n*-alkene products, which mainly focus on the hydrocarbon chain length from C₆–C₂₄. Based on the results, it was indicated that the produced liquid was mostly in alkene form rather than alkane. Under hydrogen-deficiency atmosphere, the reaction tends to remove the oxygen content via cracking (the CC bond scission), decarboxylation (CO₂), decarbonylation (CO) and also dehydration (H₂O), which shall then lead to rearrangement of molecular compounds to a more stable alkenes form [10]. Results showed that catalyst-free product (blank experiment) rendered considerable amount *n*-alkanes (12.51%) and *n*-alkenes (28.45%) of C₆–C₁₆ range. This shows that blank reaction system possess high cracking reaction but low tendency to undergo decarboxylation/decarbonylation reaction due to the low formation of C₁₇ both saturated and unsaturated compounds [35]. In contrast, Ca-based catalysts (CaO, standard nano-Ca(OH)₂ and surfactant-treated Ca(OH)₂) gave significant formation of

saturated C₁₇ and unsaturated C₁₇ hydrocarbon chain. The *n*-C₁₇ selectivity was followed the order of Ca(OH)₂–CTAB≈Ca(OH)₂–EG>Ca(OH)₂–H₂O>CaO>Ca(OH)₂–STD-nano>free-catalyst reaction. Surfactant treated Ca(OH)₂ nano-catalyst is prone to decarboxylation/decarbonylation and rendered the highest selectivity due to the presence of larger amount of surface area with large porosity, which provided a bigger sites for large molecular triolein to react. Furthermore, higher basicity of active sites from surfactant-treated Ca(OH)₂ has made the absorption of the released of CO₂ gas during deoxygenation reaction more effective and hence avoided the formation of by-product (coke). In addition, the superior properties of surfactant treated catalysts (Ca(OH)₂–CTAB and Ca(OH)₂–EG) have higher reactivity with higher yield of deoxygenated product (liquid hydrocarbon C₆–C₂₄), 47.37% and 44.50%, respectively as compared to other catalysts.

The relative activities indicator for decarboxylation/decarbonylation reactions were determined by calculating the ratio of *n*-alkanes (C_{oddnumber}) to *n*-alkanes (C_{evennumber}) of the deoxygenized product. As triolein composed mainly of C₁₈ fatty acid, thus the ratio used for calculation was *n*-C₁₇/(*n*-C₁₇+*n*-C₁₈). Based on the results, the C₁₇/(*n*-C₁₇+*n*-C₁₈) ratio was increased in the order of Ca(OH)₂–EG (0.88)>Ca(OH)₂–STD-Nano(0.85)>Ca(OH)₂–CTAB(0.75)>Ca(OH)₂–H₂O(0.68)>CaO (0.52)>free-catalyst reaction (0.42). Surfactant treated Ca(OH)₂ nanocatalyst rendered high ratio at 0.75–0.88, suggesting that triolein were deoxygenated efficiently via decarboxylation and/or decarbonylation. In contrast, low ratio of C₁₇/(*n*-C₁₇+*n*-C₁₈) indicated that the generated product were mostly in light hydrocarbon (*n*-C₈ to *n*-C₁₆). This is in agreement with selectivity study where blank reaction or CaO catalysed reaction rendered large fraction of light hydrocarbon in range of *n*-C₈ to *n*-C₁₆.

Under hydrogen deficiency condition, the decarboxylation of unsaturated oleic acid (from triolein) tends to form *n*-heptadecenes (mono-unsaturated; C₁₇H₃₄) via scission of CC bond of fatty acid (oleic acid), which leads to the oxygen removal in the form of CO₂ gas as by products. For decarbonylation reaction, di-unsaturated *n*-heptadecene (C₁₇H₃₂) was produced by removing oxygen in the form of CO gas and water as a by-product (Fig. 9) [36]. Thus, the

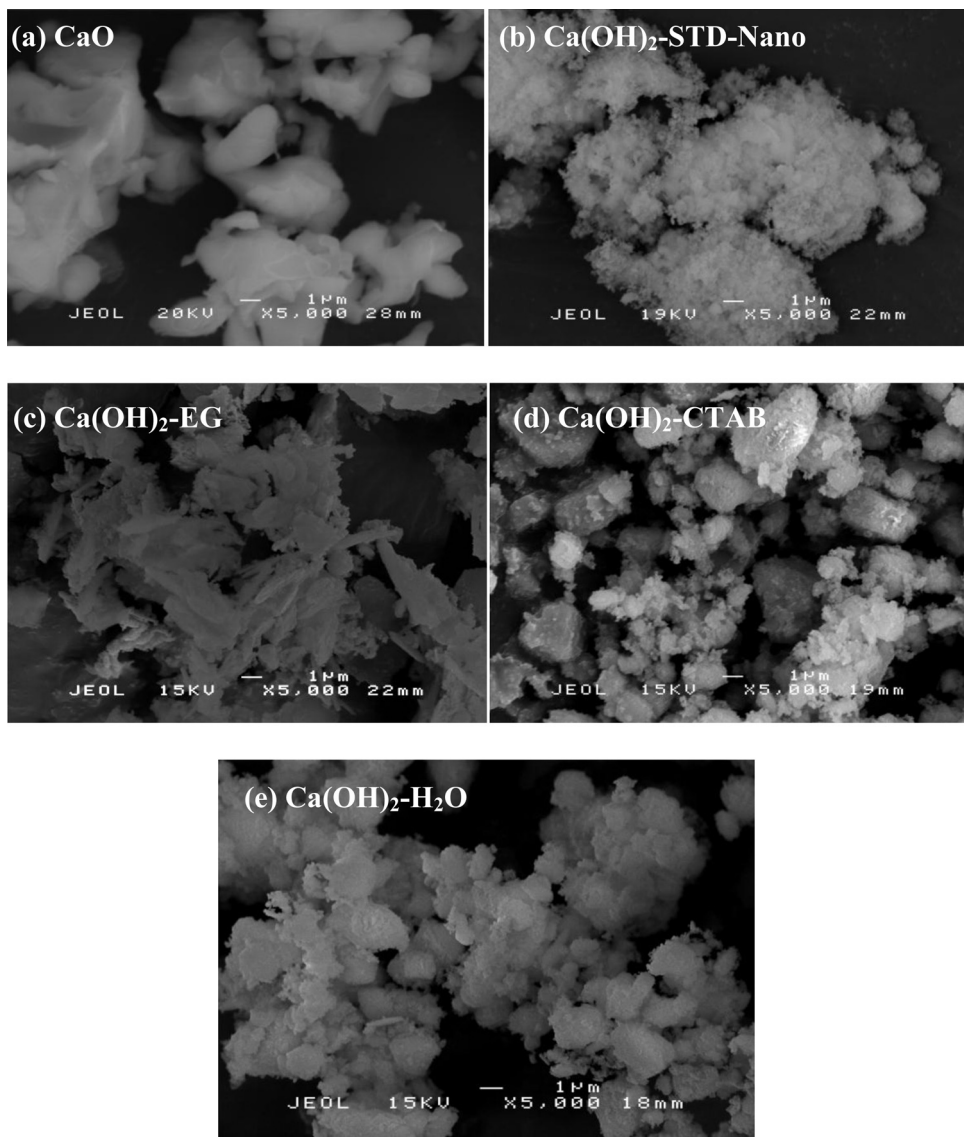


Fig. 5. SEM images of (a) CaO, (b) Ca(OH)₂-STD-Nano, (c) CS-Ca(OH)₂-EG (d) Ca(OH)₂-CTAB and (e) Ca(OH)₂-H₂O.

Table 3
Composition profile of deoxygenized product (liquid hydrocarbon).

Catalyst	Total deoxygenated product (Peak area%)	n-alkane (Peak area%)	n-alkene (Peak Area%)	Selectivity of the product obtained (Peak area%)						
		n-C ₆ -n-C ₁₆	n-C ^a =C ₁₇	n-C ^b =C ₁₇	n-C ₁₇	n-C ₁₈	n-C ₁₉ -n-C ₂₄	n-C ₁₇ /(n-C ₁₇ +n-C ₁₈)		
Blank (without catalyst)	41.13	12.51	28.62	39.96	—	—	0.29	0.4	0.31	0.42
CaO	35.86	5.28	30.58	14.26	5.50	0.2	0.70	5.83	3.34	0.52
Ca(OH) ₂ -STD-Nano	34.71	16.33	18.38	28.17	4.22	0.42	0.74	0.92	1.39	0.85
Ca(OH) ₂ -EG	47.37	12.89	34.48	29.01	9.84	0.2	—	1.34	6.34	0.88
Ca(OH) ₂ -CTAB	44.55	13.77	30.78	23.6	11.84	0.42	1.43	4.36	2.9	0.75
Ca(OH) ₂ -H ₂ O	35.70	6.85	28.85	18.01	8.52	0.16	—	3.94	3.94	0.68

Reaction parameter: reaction time: 30 min; Temperature: 350 °C; Pressure: 10 mbar.

Total deoxygenated product: liquid hydrocarbon (n-C₆-n-C₂₄).

C^a=C₁₇: mono-unsaturated C₁₇ alkene (C₁₇H₃₄).

C^b=C₁₇: di-unsaturated C₁₇ alkene (C₁₇H₃₂).

C₁₇: alkane C₁₇ (C₁₇H₃₆).

efficiency of decarboxylation or and decarbonylation using different type of catalysts can be determined by comparing the GC-MS peak area% of mono-unsaturated and di-unsaturated C17 hydrocarbon fractions that obtained from the deoxygenated product. Based

on the GC-MS results (Table 3 and Fig. 10), the higher content of C₁₇H₃₄ suggested that the decarboxylation reaction was preferred instead to the decarbonylation reaction during Ca-based catalysed reaction pathways.

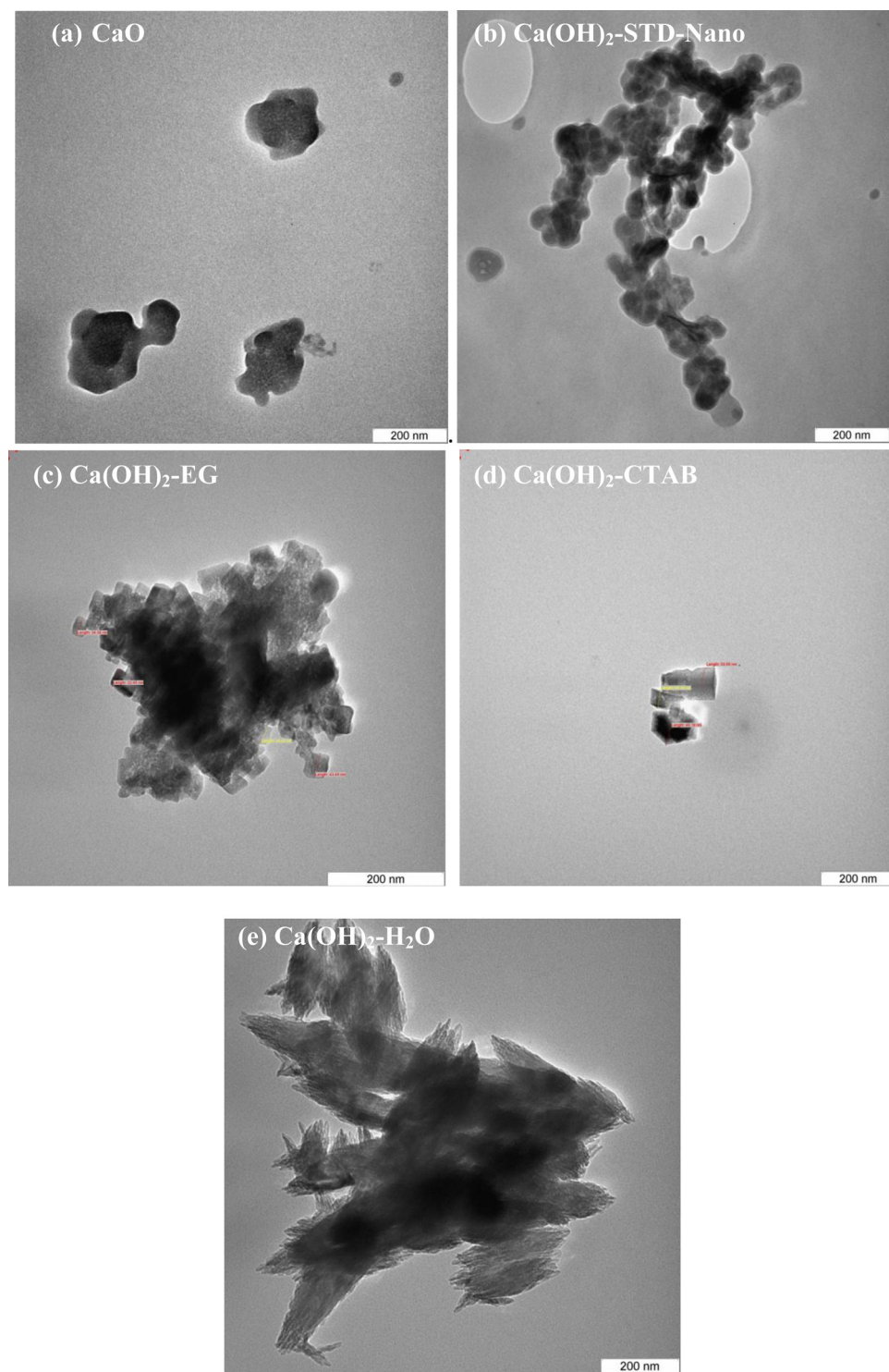


Fig. 6. TEM images of (a) CaO, (b) Ca(OH)₂-STD-Nano, (c) Ca(OH)₂-EG (d) Ca(OH)₂-CTAB and (e) Ca(OH)₂-H₂O.

4. Conclusion

The clamshell-derived catalysts (CaO and nano-Ca(OH)₂) are potential deoxygenation catalysts for the biofuel production via cracking-decarboxylation-decarbonylation pathways. The Ca(OH)₂ nanocatalyst that prepared via sonochemically assisted wet surfactant method has successfully increased of catalyst's textural

properties and surface basicity. The presence of superior properties from surfactant treated catalysts has been proven to have high selectivity of alkane and alkene in chain length of n-C₁₇ (high value of C₁₇/(n-C₁₇ + n-C₁₈) ratio). Both Ca(OH)₂-EG and Ca(OH)₂-CTAB are capable of producing higher content of liquid hydrocarbon (n-C₆-n-C₂₄) with the yield of 47.37% and 44.5%, respectively.

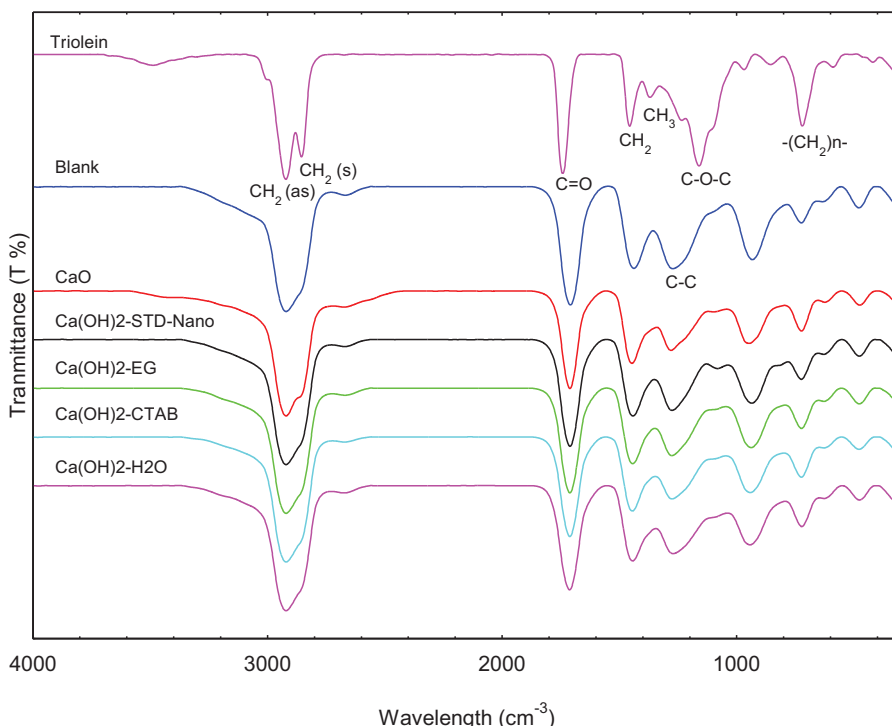


Fig. 7. FTIR results for triolein and deoxygenated products.

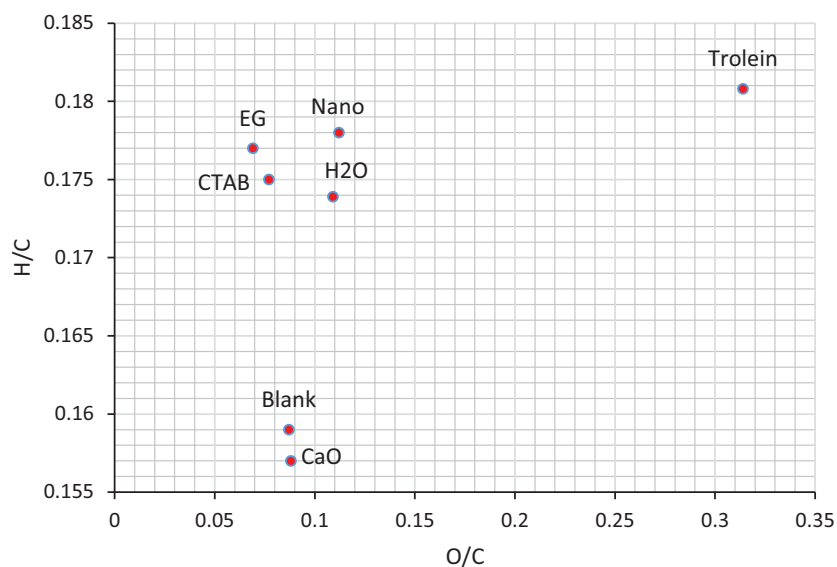


Fig. 8. H/C and O/C ratio for deoxygenized liquid product (Van Krevelen diagram).

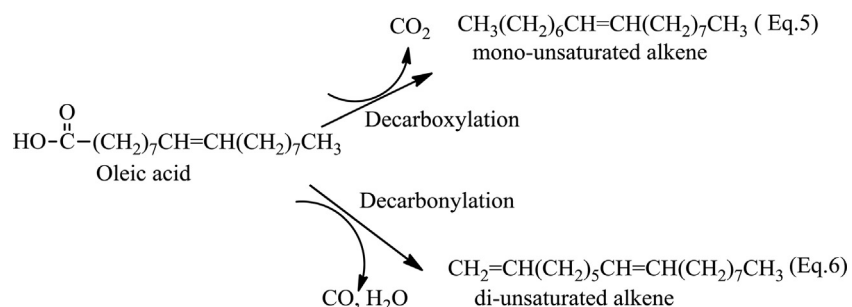


Fig. 9. Proposed mechanism for decarboxylation and decarbonylation of oleic acid.

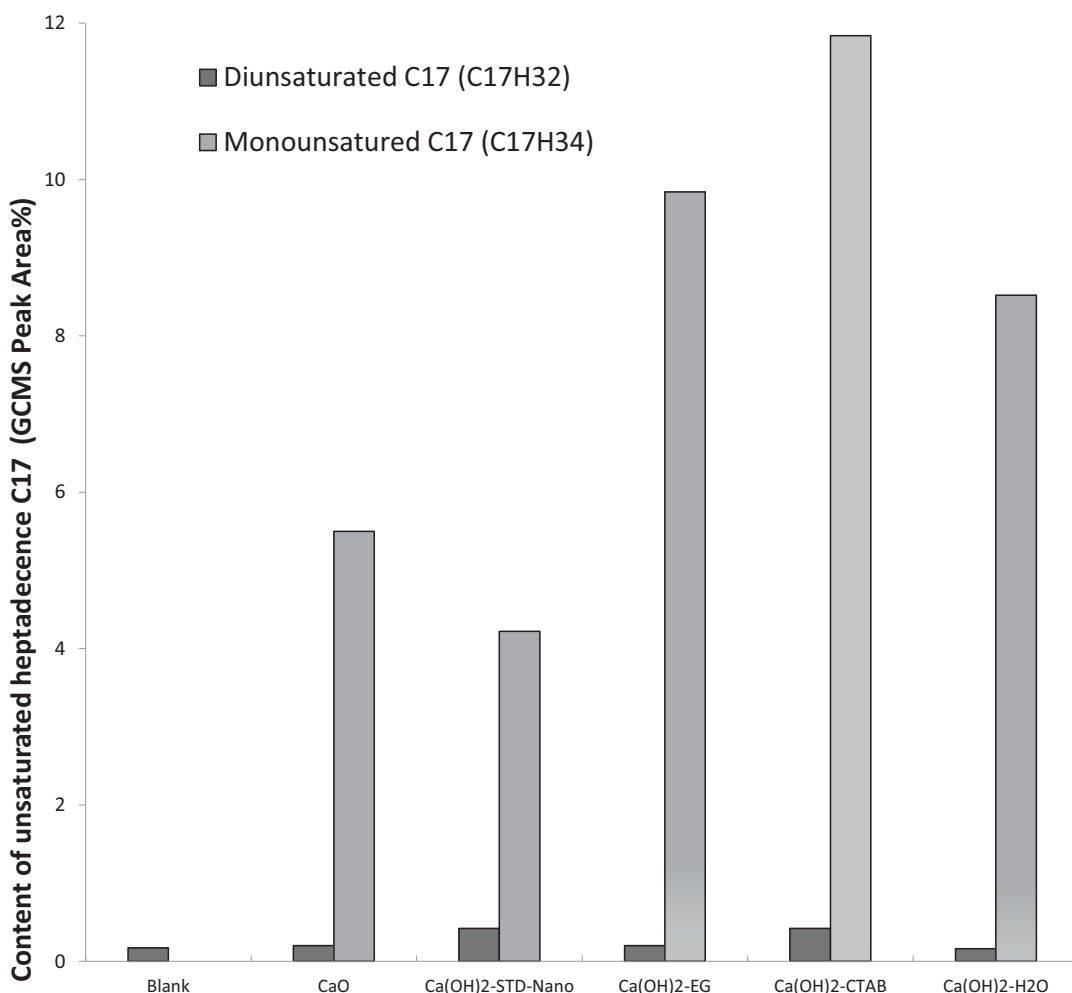


Fig. 10. Decarboxylation and decarbonylation profile for different types of Ca-based catalysed reaction.

Acknowledgements

The authors acknowledge the financial support from Ministry of Higher Education Malaysia for Fundamental Research Grant Scheme (FP056-2013B) and University Malaysia (RP025B-14AET and GC001B-14AET)

References

- [1] J.-O. Shim, D.-W. Jeong, W.-J. Jang, K.-W. Jeon, B.-H. Jeon, S.Y. Cho, H.-S. Roh, J.-G. Na, C.H. Ko, Y.-K. Oh, S.S. Han, Renew. Energy 65 (2014) 36.
- [2] D.Y.C. Leung, X. Wu, M.K.H. Leung, Appl. Energy 87 (2010) 1083.
- [3] Boeing conducts first flight using green diesel. Online at www.chicagotribune.com/business/et-boeing-green-diesel-1204-biz-20141203-story (accessed April 2015).
- [4] A.P. Vyas, J.L. Verma, N. Subrahmanyam, Fuel 89 (2010) 1.
- [5] H.-S. Roh, I.-H. Eum, D.-W. Jeong, B.E. Yi, J.-G. Na, C.H. Ko, Catal. Today 164 (2011) 457.
- [6] X. Zhang, Q. Zhang, T. Wang, L. Ma, Y. Yu, L. Chen, Bioresour. Technol. 134 (2013) 73.
- [7] M. Kleinert, J.R. Gasson, T. Barth, J. Anal. Appl. Pyrolysis 85 (2009) 108.
- [8] A. Srifa, K. Faungnawakij, V. Itthibenchapong, S. Assabumrungrat, Chem. Eng. J. (2014).
- [9] W. Mu, H. Ben, X. Du, X. Zhang, F. Hu, W. Liu, A.J. Ragauskas, Y. Deng, Bioresour. Technol. 173 (2014) 6.
- [10] I.K.k. M. Snare, P. Mäki-Arvela, D. Chichova, K. Eränen, D.Y. Murzin *, Fuel 87, (2008) 933.
- [11] E. Meller, U. Green, Z. Aizenshtat, Y. Sasson, Fuel 133 (2014) 89.
- [12] H. Shi, J. Chen, Y. Yang, S. Tian, Fuel Process. Technol. 118 (2014) 161.
- [13] C.M.R. Prado, N.R. Antoniosi Filho, J. Anal. Appl. Pyrolysis 86 (2009) 338.
- [14] J.M. Gómez, M.D. Romero, V. Callejo, Catal. Today 218 (2013) 143.
- [15] H. Tani, T. Hasegawa, M. Shimouchi, K. Asami, K. Fujimoto, Catal. Today 164 (2011) 410.
- [16] L. Ding, P. Rahimi, R. Hawkins, S. Bhatt, Y. Shi, Appl. Cata. A: Gen. 371 (2009) 121.
- [17] Y. Lin, C. Zhang, M. Zhang, J. Zhang, Energy Fuels 24 (2010) 5686.
- [18] B. Yoosuk, P. Udomsap, B. Puttasawat, Appl. Cata. A: Gen. 395 (2011) 87.
- [19] B. Yoosuk, P. Udomsap, B. Puttasawat, P. Krasae, Bioresour. Technol. 101 (2010) 3784.
- [20] N. Asikin-Mijan, Y.H. Taufiq-Yap, H.V. Lee, Chem. Eng. J. 262 (2015) 1043.
- [21] N. Asikin-Mijan, H. Lee, Y. Taufiq-Yap, Chem. Eng. Res. Des. 102 (2015) 368.
- [22] N. Viriya-Empikul, P. Krasae, B. Puttasawat, B. Yoosuk, N. Chollacoop, K. Faungnawakij, Bioresour. Technol. 101 (2010) 3765.
- [23] J.A. Botas, D.P. Serrano, A. García, J. de Vicente, R. Ramos, Catal. Today 195 (2012) 59.
- [24] Q. Lu, Z. Tang, Y. Zhang, X.-f. Zhu, Ind. Eng. Chem. Res. 49 (2010) 2573.
- [25] M.-J. Jeon, S.-S. Kim, J.-K. Jeon, S.H. Park, J.M. Kim, J.M. Sohn, S.-H. Lee, Y.-K. Park, Nanoscale Res. Lett. 7 (2012) 1.
- [26] M.J. Romero, A. Pizzib, G. Toscanob, B. Bosioa, E. Arato, Chem. Eng. 37 (2014).
- [27] P. Duan, X. Bai, Y. Xu, A. Zhang, F. Wang, L. Zhang, J. Miao, Fuel 109 (2013) 225.
- [28] J.A. Jacob, S. Kapoor, N. Biswas, T. Mukherjee, Colloids Surf. A: Physicochem. Eng. Aspects 301 (2007) 329.
- [29] S. Nam, D.V. Parikh, B.D. Condon, Q. Zhao, M. Yoshioka-Tarver, J. Nanopart. Res. 13 (2011) 3755.
- [30] A. Javidan, A. Ziari, J. Safaei-Ghom, Ultrason. Sonochem. 21 (2014) 1150.
- [31] H.V. Lee, J.C. Juan, N.F. Binti Abdullah, R. Nizah Mf, Y.H. Taufiq-Yap, Chem. Cent. J. 8 (2014) 30.
- [32] NBB., (2009).
- [33] H.V. Lee, Y.H. Taufiq-Yap, M.Z. Hussein, R. Yunus, Energy 49 (2013) 12.
- [34] J. Salimon, N. Salih, B.M. Abdullah, BioMed Res. Int. 2011 (2011).
- [35] S.K. Kim, S. Brand, H.-s. Lee, Y. Kim, J. Kim, Chem. Eng. J. 228 (2013) 114.
- [36] M. Snare, I. Kubickova, P. Mäki-Arvela, K. Eränen, D.Y. Murzin, Ind. Eng. Chem. Res. 45 (2006) 5708.